

# Phylogenetic quantification of intra-tumour heterogeneity

Roland F Schwarz<sup>\*1,2,3</sup>, Anne Trinh<sup>1,2</sup>, Botond Sipos<sup>3</sup>, James D Brenton<sup>1,2,4</sup>, Nick Goldman<sup>3</sup>, Florian Markowetz<sup>\*1,2</sup>

<sup>1</sup>University of Cambridge, Cambridge UK

<sup>2</sup>Cancer Research UK Cambridge Institute, Cambridge, UK

<sup>3</sup>European Bioinformatics Institute, Hinxton, UK

<sup>4</sup>Department of Oncology, University of Cambridge, UK

Email: Roland F Schwarz - rfs32@cam.ac.uk; Anne Trinh - anne.trinh@cruk.cam.ac.uk; Botond Sipos - sbotond@ebi.ac.uk; James Brenton - james.brenton@cruk.cam.ac.uk; Nick Goldman - goldman@ebi.ac.uk; Florian Markowetz - florian.markowetz@cruk.cam.ac.uk;

\*Corresponding author

## Abstract

---

**Background:** Intra-tumour heterogeneity (ITH) is the result of ongoing evolutionary change within each cancer. The expansion of genetically distinct sub-clonal populations may explain the emergence of drug resistance and if so would have prognostic and predictive utility. However, methods for objectively quantifying ITH have been missing and are particularly difficult to establish in cancers where predominant copy number variation prevents accurate phylogenetic reconstruction owing to horizontal dependencies caused by long and cascading genomic rearrangements.

**Results:** To address these challenges we present MEDICC, a method for phylogenetic reconstruction and ITH quantification based on a **Minimum Event Distance for Intra-tumour Copynumber Comparisons**. Using a transducer-based pairwise comparison function we determine optimal phasing of major and minor alleles, as well as evolutionary distances between samples, and are able to reconstruct ancestral genomes. Rigorous simulations and an extensive clinical study show the power of our method, which outperforms state-of-the-art competitors in reconstruction accuracy and additionally allows unbiased numerical quantification of ITH.

**Conclusions:** Accurate quantification and evolutionary inference are essential to understand the functional consequences of ITH. The MEDICC algorithms are independent of the experimental techniques used and are applicable to both next-generation sequencing and array CGH data.

---

## Background

The study of intra-tumour genetic heterogeneity (ITH) is now a major focus of cancer genomics research [1–12] due to its potential to provide prognostic information [13–15] and to explain mechanisms of drug resistance [16–19]. Quantifying heterogeneity and understanding its aetiology crucially depends on our ability to accurately reconstruct the evolutionary history of cancer cells within each patient. In many cancers, such as high-grade serous ovarian cancer (HGSOC), most of this heterogeneity is not reflected in point mutations but in genomic rearrangements and endoreduplications that lead to aberrant copy number (CN) profiles [20, 21]. In these cases tree inference is hindered by unknown phasing of parental alleles, horizontal dependencies between adjacent genomic loci and the lack of curated CN profile databases to use as a reference for probabilistic inference. Therefore heterogeneity and evolutionary divergence are typically quantified using ad-hoc thresholds [19] and tree inference is often done subjectively [11]. Approaches developed to address this problem include Greenman et al. [22], a graph theoretical approach on signed reversals to order rearrangement events, but this requires detailed annotation of rearrangements in the data that may not be available, and the algorithm does not generally infer global trees representing cancer evolution within a patient. The *TuMult* algorithm [23] deals with underlying computational complexity by considering only breakpoints — locations on the genome where the CN changes — and by using total CN without phasing of parental alleles. While simplifying the computational problem, this approach discards potentially informative data.

Our aim is to establish numerical quantification of ITH per patient from CN profiles that can routinely be acquired from clinical samples. To this end, we have developed MEDICC (Minimum Event Distance for Intra-tumour Copy-number Comparisons), a method for accurate inference of phylogenetic trees from unsigned integer CN profiles. MEDICC specifically addresses the following challenges associated with CN-based phylogeny estimation. i) It makes use of the full CN information across both parental alleles by estimating an optimal *phasing* of CN variants using the evolutionary information. ii) It deals with *horizontal dependencies* between adjacent genomic loci and with multiple overlapping events by using efficient heuristics. It can therefore work on complete genomic profiles instead of breakpoints which allows the reconstruction of ancestral genomes. iii) It implements statistical tests for evolutionary rates, tests for

phylogenetic structure and tests for the relationship between clonal subpopulations to provide informative *summary statistics* for the reconstructed evolutionary histories and ITH.

We developed MEDICC and successfully applied it to the analysis of a novel dataset of 170 CN profiles of patients undergoing neo-adjuvant chemotherapy for HGSOc as described in our accompanying clinical study (Schwarz *et al.* 2013 *in prep.*). In the following we first give a more detailed description of the data and problems that MEDICC addresses. We then introduce the MEDICC modelling framework that guides all steps of the algorithm and which is then explained in detail. We finish with a demonstration of MEDICC on a real-world example of a case of endometrioid cancer and give simulation results that compare it to competing methods.

## Results and Discussion

MEDICC was designed to work on human integer CN profiles that can routinely be obtained from single nucleotide polymorphism (SNP) arrays [24] or paired-end sequencing [25, 26]. In both cases DNA content is quantified relative to a diploid normal in windows along the genome. Point mutations help to distinguish the two parental alleles and the resulting profile comprises two vectors of integer CNs, representing the absolute number of copies of that particular genomic segment in both alleles; however the *phasing* of those CNs to the two parental alleles is unknown, unless two SNPs happen to be on the same read or other external linkage information is available [11]. Consequently, by definition (and for each genomic segment independently), the larger of the two CNs is termed the *major* and the other the *minor* CN, without any information about which CNs belong together on the same allele (Figure 1 left). Without resolving this ambiguity, tracing of individual events is not possible.

Another challenge is horizontal dependency in CN profiles. In contrast to nucleotide substitution models where sites in a sequence are modelled as independent and identically distributed (iid) [27], CN events often overlap and range across many adjacent genomic regions and thereby introduce horizontal dependencies that influence estimation of evolutionary divergence.

Given multiple such evolutionarily-related CN profiles, for example from distinct primary and metastatic sites of the same patient, phylogenetic inference in MEDICC then involves three steps: (i) allele-specific assignment of major and minor CNs, (ii) estimation of evolutionary distances between samples followed by tree inference and (iii) reconstruction of ancestral genomes (Figure 1). All three steps are guided by a minimum evolution criterion. Similar to early edit-distances for sequence analysis [28], MEDICC counts the number of genomic events needed to transform one CN profile into another and searches for the tree

that minimises this criterion.

### **MEDICC reconstructs evolutionary histories via a minimum evolution criterion**

We model the evolution of genomic rearrangements through the following set of events that have an observable effect on CN profiles: terminal and interstitial deletions, as well as unbalanced translocations, are single deletion events; tandem and inverted duplications are single amplification events; and breakage fusion bridges are dual events involving a duplication and a deletion [22]. We use a finite-state automaton representation of genomic profiles and finite-state transducers [29] for modelling and efficient computing of the minimum-event distance based on these genomic events (Figure 2A). Before going through the three steps of the reconstruction process in detail it is necessary to introduce some terminology; for a more thorough introduction into transducer theory see [29–31] and references therein.

#### *The MEDICC modelling framework*

MEDICC models diploid genomic CN profiles as sequences over the alphabet  $\Sigma = \{0, \dots, K, "X"\}$ , where  $\{0, \dots, K\}$  represent integer CNs ( $K$  is the maximum haploid CN) and “X” is a special character that separates the two alleles on which events can happen independently. For example, the profile 1123002X0122002 represents a chromosome with 7 regions distinguished, with the first region present in one copy on one allele and absent in the other allele; the second region present in one copy on each allele; and so on up to the seventh region present in two copies on each allele. This means that MEDICC deals with a maximum total CN of  $2K$  in a diploid genome. By default  $2K = 8$  which is the upper end of the dynamic range of SNP arrays, but the alphabet can be extended easily without changing the implementation. In this manuscript the terms “sequence” and “(CN) profile” are used interchangeably. CN profiles are implemented as acceptors, weighted finite-state automata (FSA) that can contain a single or multiple such profiles. The minimum-event distance is implemented as a weighted finite-state transducer (FST, [29]). FSTs are an extension of FSAs with input and output symbols — like pair-HMMs they emit or accept two sequences simultaneously, meaning they model the events transforming on sequence into another. Both FSAs and FSTs can be equipped with weights from a semiring, enabling calculations to be weighted according to some importance criterion. One of the most common semirings is the real semiring (e.g. the weights represent probabilities), where weights are multiplied along a path in the automaton and the total weight of a sequence (or pair of sequences) is the sum (total probability) over all possible paths generating that sequence. Equally popular is the tropical semiring, also known as the Viterbi path, where

weights are summed along a path and the total weight is the minimum across all those paths. In this case weights are often “penalties” or negative log-probabilities for taking a certain path, similar to classical pairwise sequence alignment in which mismatches and indels are penalised with additive fixed scores. MEDICC uses the tropical semiring for computing the minimum event distance, but the modularity of the framework allows us to smoothly transition to probabilities at a later stage by switching semirings without changing the algorithm. In this tropical semiring a FST  $T_1$  then assigns a score to two sequences (represented as acceptors)  $x$  and  $z$  via

$$T_1[x, z] = \min_{p \in P} \sum_i w(p, i).$$

where  $P$  is the set of all possible paths through the FST in which the input and output symbols match with the sequences  $x$  and  $z$  and  $w(p, i)$  is the weight of that path at position  $i$  in the sequence. No score is returned for a pair of sequences for which no valid path in  $T_1$  exists. This leads to the definition of the minimum-event distance, which governs all three steps of the reconstruction process.

### *Constructing the minimum-event distance for CN profiles*

Figure 2B shows the one-step transducer  $T_1$  that we use to model single amplifications and deletions of arbitrary length and that counts one event each time the amplification or deletion state is entered. This is analogous to an affine gap cost model in classical sequence alignment [32].  $T_1[x, z]$  therefore assigns to each pair of sequences  $(x, z)$  the minimum number of events necessary to transform one sequence into another. At this point, however, not all possible CN scenarios have a valid path (e.g. one event can amplify “1” to “2” but not “1” to “3”). To include all possible changes across multiple events,  $T_1$  is composed  $K$  times with itself [30]. In essence, composition describes the chaining of FSTs, where the total weight of the composed transducer is the total minimum score from the input sequence  $x$  via intermediate sequences  $y_i$  to the target sequence  $z$ :

$$\begin{aligned} T[x, z] &= (T_1 \circ \dots \circ T_1)[x, z] \\ &= \min_{y_1, \dots, y_{K-1}} (T_1[x, y_1] + \dots + T_1[y_{K-1}, z]) \end{aligned}$$

This gives rise to the FST  $T$  that strictly adheres the modelled biological constraints such as no amplification from zero. We call  $T$  the *tree* transducer: these biological constraints give it a direction, and it is not guaranteed to return a distance for any pair of CN profiles.

As we are interested in the minimum evolutionary distance between any two sequences  $x$  and  $z$  via their last common ancestor (LCA)  $y$ , the final distance FST  $D$  is formed by composing  $T$  with its inverse (Figure 2C, [33]), such that  $D$  computes the distance from a leaf node to the LCA ( $T^{-1}$ ) and back ( $T$ ) to the other leaf node:

$$\begin{aligned} D[x, z] &= (T^{-1} \circ T)[x, z] \\ &= \min_y (T^{-1}[x, y] + T[y, z]) \end{aligned}$$

In the real semiring, and equipped with probabilities, this would be analogous to classical phylogenetic reconstructions where a reversible model of sequence evolution is used to compute the likelihood of the subtree containing sequences  $x$  and  $z$  as the products of the individual likelihoods of seeing  $x$  and  $z$  given their ancestor  $y$  and summing over all  $y$  [34]. In our case,  $D$  equivalently computes the minimum number of events from  $x$  to  $z$  via their LCA. This distance is symmetric and is guaranteed to yield a valid distance for any pair of sequences. In the rest of the paper, “distance” refers to this minimum-event distance, unless stated otherwise.

MEDICC therefore computes an evolutionary distance between two genomes based on a minimum evolution criterion via their closest possible LCA. Due to composition of the tree transducer  $T$  with its inverse, the resulting distance  $D$  is a dissimilarity score that represents (the logarithm of) the shortest-path approximation to a positive-semidefinite kernel score [35, 33]. This means that computing the evolutionary distances between samples automatically places these samples in a high-dimensional evolutionary space, where in addition to distances we gain information about their relative position and angles. We term this space the mutational landscape, on which we can directly apply explorative analyses like PCA, classification with support-vector machines and other machine learning techniques [36]. We use *OpenFST*, an efficient implementation of transducer algorithms [37] to achieve exact distance computation in quadratic time. Following the minimum evolution principle, the overall objective is to find a tree topology including ancestral states that minimises the total tree length, i.e. the total number of genomic events along the tree. In the following we will describe how MEDICC achieves this in its three step process.

### *Step 1: Evolutionary phasing of major and minor CNs*

As CN-changing events can independently occur on either or both of the parental alleles, the allele-specific assignment, or phasing, of major and minor CNs heavily influences the minimum tree length objective. We

use the evolutionary information between samples to solve these ambiguities. Using our distance measure we can choose an optimal phasing between a pair of diploid profiles that minimises the pairwise distance between them (Figure 3A). This respects the distinct evolutionary histories of both alleles and finds a phasing scenario in which the evolutionary trajectories between both haploid pairs are minimal. To achieve this, a diploid profile is represented as a single sequence in which the allele boundaries are marked by a separator character as described above. From each pair of major and minor input sequences we can generate up to  $2^L$  such concatenated sequences, where  $L$  is the length of the input profile (both alleles have the same length). This number is too large to enumerate exhaustively, so in order to achieve a compact representation of diploid profiles we make use of a context-free grammar (CFG). Our implementation is related to the use of CFGs to model RNA structures, where paired residues in stem regions are not independent [32].

In our CN scenario a CFG represents different allele phasing choices (see Figure 3B right). At every position in the diploid profile we have a choice of using the major as the first allele and the minor as the second or (“”) vice versa (Figure 3B left). Each possible parse tree of the CFG then corresponds to one phasing scenario out of the  $2^L$  possibilities. When the distance FST reads the separator it is forced to return to the match state (initial state), thus guaranteeing that the total distance to another profile equals the sum of the distances of the two alleles with no events spanning different alleles. We represent CFGs algorithmically by pushdown-automata in the FST library [38].

While this approach works well for finding phasing scenarios that minimise the distance between one pair of profiles, we aim to find phasing scenarios that jointly minimise the distances between all profiles in the dataset. To reduce the computational complexity of this task it is necessary to employ a heuristic.

MEDICC searches for the single profile that has minimum sum of distances to all sample profiles, that is, the geometric median, through an iterative search. This centre profile is then compared again to each individual profile and the shortest path algorithm yields the choice of phasing that minimises the distance between each profile and the centre. While this is not guaranteed to return a globally optimal phasing scenario, it has proven to perform very well in practise.

### *Step 2: Distances and tree reconstruction*

Once the alleles have been phased, pairwise evolutionary distances between samples can be computed as the sum of the pairwise distances between both alleles. MEDICC then uses the Fitch-Margoliash algorithm [39] for tree inference from a distance matrix with or without clock assumption. A test of clock-like events,

available using functionality in the accompanying R package *MEDICCquant*, allows us to determine which tree reconstruction algorithm is most appropriate (see the section on quantification of ITH).

### *Step 3: Ancestral reconstruction and branch lengths*

From this point on we keep the topology of the tree fixed, and traverse from its leaves to the root to infer ancestral CN profiles and branch lengths. Ancestral reconstruction is possible because cancer trees are naturally rooted by the diploid normal from which the disease evolved. Reconstructing ancestral genomes allows us to investigate e.g. the genomic makeup of the cancer precursor, the LCA of all cancer samples in the patient. Events that across patients frequently occur between the root of the tree and the precursor are likely driver events of cancer progression. Ancestral reconstruction also determines the final branch lengths of the tree. MEDICC infers ancestral genomes for each allele independently using a variant of Felsenstein's Pruning algorithm [27]. In traditional ancestral reconstruction the total score (likelihood/parsimony score) of the tree is computed in a downward pass towards the root and ancestral states are then fixed in a second upward pass, successively choosing the most likely/most parsimonious states.

In our scenario, the algorithm begins by composing each of the  $n$  terminal nodes with the tree transducer  $T$ , which yields  $n$  acceptors holding all sequences reachable from that terminal node and their respective distances. When the first two terminal nodes are joined in their LCA the corresponding acceptors are intersected. The resulting acceptor contains only those profiles that were contained in both input acceptors and their corresponding weights are set equal to the sum of the weights of the profiles in the input acceptors. In a probabilistic framework the resulting acceptor is equivalent to the conditional probability distribution  $P(\text{subtree}(x, z) \mid \text{LCA } y) = P(x|y)P(z|y)$  for each possible LCA, where the sum of distances again is replaced by the product of the conditional probabilities of seeing a leaf node given its ancestor. This intersection will still contain the vast majority of all possible profiles, but each with a different total distance, and without those that are prohibited by biological constraints. For example, the ancestor cannot have a CN of zero at a position where at least one of its leaf nodes has  $\text{CN} > 0$ , as amplifications from zero are not allowed.

Because after phasing each leaf node is represented by an acceptor containing exactly one diploid sequence, computing this set of possible ancestors is computationally feasible. However, because during tree traversal we need to compose these sets of possible profiles repeatedly with the tree transducer  $T$ , the result would increase in size exponentially because it has to account for all possible events of arbitrary length at each position in all sequences. Therefore during tree traversal, when two internal nodes have to be joined in



their LCA, MEDICC reduces them to a single sequence by choosing those two sequences with smallest distance to each other. This fixes the profiles for those two internal nodes. This procedure is continued until all internal nodes are resolved. Once all ancestral CN profiles have been reconstructed the final branch lengths are simply the distances between the nodes defining that branch in the tree.

### **MEDICC improves phylogenetic reconstruction accuracy**

We assessed reconstruction accuracy using simulated data generated by the *SimCopy* R package [40] (see Methods). Random coalescent trees were generated with *APE* [41]. To create an unbiased simulation scenario, genome evolution was simulated using increasing evolutionary rates on the sequence level using five basic genomic rearrangement events: deletion, duplication, inverted duplication, inversion and translocation (for details see Methods). Once the simulations were complete, CNs were counted for each genomic segment and these CN profiles were used for tree inference using the following three methods: i) BioNJ [42] tree reconstruction on a matrix of euclidean distances computed directly on the CNs, ii) breakpoint-based tree-inference using the *TuMult* software [23] and iii) MEDICC. *TuMult* additionally requires array log-intensities as input. In order to keep the comparisons unbiased, noiseless log ratios simulating CGH array intensities for *TuMult* were directly computed from the CN profiles. To assess the relative abilities of the methods to correctly recover the evolutionary relationships of the simulated CN profiles, reconstruction accuracy was measured in quartet distance [43] between the true and the reconstructed tree. Quartet distance was chosen as it only considers topological differences; branch lengths have widely different meanings in the methods tested and as such are not comparable.

This simulation strategy is based on basic biological principles, independent of the methods compared and *a priori* does not favour any of them. All simulations were repeated to cover a wide parameter range, yielding qualitatively similar results.

The simulation results clearly show the improvement in reconstruction accuracy of MEDICC over naive approaches (BioNJ on Euclidean distances) and competing methods (*TuMult*) (Figure 4A). In general, reconstruction accuracies increase with increasing evolutionary rates. Especially when the amount of phylogenetic information is limited, MEDICC outperforms other methods by a significant margin. This may be because of two reasons: firstly, in contrast to other methods MEDICC is capable of phasing the parental alleles, thereby making much more effective use of the phylogenetic information compared to methods that work on total CN alone. Secondly, due to efficient and accurate heuristics, MEDICC can deal with the horizontal dependencies imposed by overlapping genomic events of arbitrary size and accurately

computes distances between them.

### **Evolutionary comparisons with MEDICC allow quantification of tumour heterogeneity**

As described earlier, the matrix of pairwise distances inferred by MEDICC is the logarithm of a rational kernel matrix [35, 33] which maps samples to a high-dimensional mutational landscape. We reduce the dimensionality of this landscape through kernel principal components analysis [44] where we can use spatial statistics to derive numerical measures of ITH for each patient.

Intra-tumour heterogeneity is a loose concept that describes the amount of genomic difference between multiple cells or samples of the same tumour. Two types of heterogeneity often of interest are *spatial* and *temporal* heterogeneity. For example, spatial differences might be observed from separate biopsies of a primary cancer and a distant metastasis. Other changes may occur between different time points, for example before and after chemotherapy. Average distances between subsets of samples might be computed by any method that returns dissimilarities between samples by simple averaging. However, as clinical datasets are noisy, more robust measures of distances between aggregated subsets of samples are desirable.

#### *Temporal heterogeneity*

We define temporal heterogeneity as the evolutionary distance between the average genomic profiles between any two time points (e.g. at biopsy before chemotherapy and at surgery after chemotherapy in the case of neo-adjuvant treatment). In the mutational landscape (see above) we are able to directly compute the centre of mass of a set of genomic profiles (which would not be possible by working with distances alone). We can then define temporal heterogeneity as the distance between the centres of mass of the samples from those two time points (Figure 5D). The advantage of this approach is that we can use robust measures of the centre of mass (e.g. ignoring the single most distant point) to estimate temporal heterogeneity. It should be noted that this general approach can be used for determining distances between any partitions of the samples in the dataset, for example between groups of samples taken from different organs as a measure of spatial heterogeneity.

#### *The clonal expansion index*

Other complex aspects of ITH that cannot be easily derived from distances alone include the ability of a tumour to undergo clonal expansions [16]. The model here is that if the majority of cancer cells are subject to strong selection pressure, such as from chemotherapy, minor subclones with a distinctive selective

advantage may repopulate. This subpopulation would be expected to coalesce early and will show a greater than expected divergence (relative to neutral evolution) from other remaining clones. This model is similar to analyses of clonality in bacterial populations [45]. Traditional tests for deviation from a neutral coalescent are typically based on single polymorphic sites and often require information about the number of generations [46]. As such information is not available for clinical cancer studies, we therefore make a spatial argument about clonal expansions. We assume that due to the large population sizes of cancer cells, genetic drift is not significant. In a setting of neutral evolution where all sequences have essentially the same fitness, sequences randomly move across the mutational landscape leading to a uniform distribution of sequences in that space (Figure 5A) with no selective sweeps or clonal expansions. On the contrary, if strong selective pressure favours specific mutations (Figure 5B), sequences are more likely to survive and be sampled from the favoured regions leading to local clustering of sequences on the mutational landscape (Figure 5C).

Besag’s  $L(r)$  [47], a variance-stabilised transformation of Ripley’s  $K(r)$ , [48] is a function used in spatial statistics to test for non-homogeneity, i.e. spatial clustering, of points in a plane.  $\lambda K(r)$  describes the expected number of additional random points within a distance  $r$  of a typical random point of an underlying Poisson point process with intensity  $\lambda$ . The empirical estimate of Ripley’s  $K$  for  $n$  points with pairwise distances  $d_{ij}$  and average density  $\hat{\lambda}$  is defined as

$$\hat{K}(r) = \frac{1}{\hat{\lambda}n} \sum_{i \neq j} I(d_{ij} < r),$$

where  $I$  is the indicator function. In case of complete spatial randomness (CSR), the expectation of  $K(r)$  is  $\pi r^2$ . Besag’s  $L$  is the transformation  $L(r) = \sqrt{K(r)/\pi}$  thereof and is under CSR in expectation linear in  $r$ . Therefore plotting  $r - \hat{L}(r)$  can be used as a graphical indication of deviation from CSR. We use a simulation approach to estimate significance bands for  $L(r)$  [49].

The clonal expansion index CE for a dataset (typically samples taken from a single patient) is then defined as the maximum ratio between the distance of the observed L-value ( $L_o(r)$ ) and the theoretical L-value under CSR ( $L_t(r)$ ) and one-half the width of the two-sided simulated significance band  $C(r)_u$  ( $u$  for upper significance band):

$$CE = \max_r \left( \frac{|L_o(r) - L_t(r)|}{C_u(r) - L_t(r)} \right) \quad (1)$$

A value of  $CE < 1$  therefore suggests CSR in the point set, whereas a  $CE$  value  $> 1$  indicates local spatial

clustering. We conducted coalescence simulations to confirm that the clonal expansion index distinguishes between trees with normal and elongated branch lengths between populations (black and red distributions, Figure 4B).

#### *Testing for star topology and molecular clock*

Tree reconstruction methods may include positive or negative assumption of a molecular clock which will significantly influence the reconstruction accuracy. It is of particular interest in cancer biology whether evolution is governed by constant or changing rates of evolutionary change. Furthermore, it is still debated whether disease progression follows a (structured) tree-like pattern of evolution or if subpopulations are emitted in radial (star-like) fashion from a small population of stem-like progenitors (see [50]).

We implement two tests for tree-likeness and molecular clock in the *MEDICCquant* package to help answer these questions. We model genomic events  $x$  as generated from a Poisson process with rate  $\rho$ . The expected number of events is then linear in time:  $E[X] = \rho t$ . Assuming  $\rho = 1$ , where the process is not time-calibrated, the observed distance  $\hat{X}$  is the maximum likelihood estimate (MLE) for the time of divergence. Under asymptotic normality of the MLE we have that  $\hat{X} \sim N(X, X)$ . Given a star topology we find optimal branch lengths that minimise the residual sum of squares between the optimised distances  $x_i^{\text{opt}}$  and the measured pairwise distances  $\hat{X}_i$  for branch  $i$ . Under the null hypothesis of star-like evolution this sum of squares

$$RSS_{\text{star}} = \sum_{i=1}^{n(n-1)/2} \frac{(x_i^{\text{opt}} - \hat{X}_i)^2}{\sqrt{\hat{X}_i}}$$

is then  $\chi^2$ -distributed with  $n(n-1)/2 - n$  degrees of freedom, where  $n$  is the number of samples studied, i.e. the number of leaves in the tree (Tim Massingham, pers. communication).

An analogous procedure can be used for testing whether a tree follows a molecular clock hypothesis, in which it exhibits constant evolutionary rates along all branches. In this case the distances of all leaf nodes from the diploid should be the same. We measure the deviation of the branch lengths from the diploid from their mean ( $\mu(\hat{X})$ ) by

$$RSS_{\text{clock}} = \sum_{i=1}^n \frac{(\mu(\hat{X}) - \hat{X}_i)}{\sqrt{\hat{X}}}$$

Because branch lengths do not need to be optimised to a specific topology, and we are only considering distances to the diploid, the distribution in this case has  $n - 1$  degrees of freedom.

### Progression and heterogeneity in a case of metastatic endometrioid adenocarcinoma

In the following section we demonstrate MEDICC on a case from the CTCR-OV03 clinical study [51]. This case had advanced endometrioid ovarian carcinoma and was treated with platinum-based neoadjuvant chemotherapy. After three cycles of chemotherapy the patient had stable disease based on RECIST assessment, pre- and post-chemotherapy CT imaging and a 92% reduction of the tumour response marker CA125. She then underwent interval debulking surgery but had residual tumour of > 1cm at completion. After six months she progressed with platinum-resistant disease and died one month later.

Out of 20 biopsy samples 18 satisfied quality control for > 50 tumour cellularity and array quality. The dataset included 14 omentum samples, two samples from the vaginal vault (VV) and two samples from the external surface of the bladder (BL). The BL and VV samples were taken prior to chemotherapy and the omental samples were collected at interval-debulking surgery after three cycles of chemotherapy.

All samples were CN profiled with Affymetrix SNP 6.0 arrays and segmented and compressed using PICNIC [24] and CGHregions [52]. Pairwise evolutionary distances between all samples were estimated with MEDICC. The distance distribution was tested for the molecular clock hypothesis using MEDICCquant and showed strong non-clock like behaviour ( $p = 2.89 \times 10^{-14}$ , Figure 6A). Tree reconstruction was performed by MEDICC using the Fitch-Margoliash algorithm [39]. MEDICCquant detected a high degree of clonal expansion ( $CE = 1.24$ ) as can be seen in the strong spatial clustering of samples on the mutational landscape (Figure 6B). MEDICC counted a median of 204 genomic events relative to the diploid and a median of 146 between all pairwise comparisons. Tree reconstruction showed good support values for the omental and BL/VV subclades, suggesting strong spatial heterogeneity. The patient also showed strong temporal heterogeneity, as there were large evolutionary distances between samples before and after neoadjuvant chemotherapy (temporal heterogeneity index 3.78, Figure 6B).

However, temporal and spatial heterogeneity in this case are indistinguishable because the BL/VV samples coincide with the biopsy samples, whereas all omentum samples were taken at surgery.

Ancestral reconstructions using MEDICC showed loss-of-heterozygosity (LOH) events on chromosome 17q (see internal node profiles in Figure 6A) that often coincide with deleterious mutations in BRCA2 and TP53 [53]. The most prominent contributors to the clonal expansions of the subgroup surrounding sample S01 seemed to be chromosomal amplifications on chromosomes 6, 8, 11 and 14; as well as LOH on chromosome 15. We also detected large LOH events on chromosomes 4, 5, 9, 10, 13, 14, 16 and 17 (Figure 6C).

## Conclusions

While significant progress has been made recently to understand tumour heterogeneity through extensive multiple sampling studies and experimental efforts, few algorithms have been developed to target the specific questions raised by such datasets. MEDICC is our contribution to better reconstruct the evolutionary histories of cancer within a patient and propose unbiased quantification of heterogeneity and the degree of clonal expansion.

We have shown the success of these efforts in simulations and their utility in the example discussed in this article. Further examples that also elaborate on the connection between clonal expansion and heterogeneity and patient outcome can be found in our extensive clinical study (Schwarz et al 2013, in prep.).

As discussed above we attribute the increase in reconstruction accuracy mainly to two factors. First, MEDICC makes efficient use of the available phylogenetic information by phasing parental alleles using the minimum evolution criterion, which has to our knowledge not been attempted before. Second, MEDICC models actual genomic events that change CN and incorporates biological constraints such as loss-of heterozygosity, which is not the case in breakpoint-based approaches.

The loss of reconstruction accuracy of *TuMult* relative even to naive approaches using Euclidean distances is most likely due to the fact that *TuMult* was designed for fewer leaf nodes (typically around 4, *Letouze, personal communication*). It is worth stressing that, unlike its competitors, MEDICC is not linked to a specific data collection platform. Data from SNP arrays can be used, as well as sequencing-based datasets or any other method that returns absolute copy numbers.

Future work will focus on reductions of algorithmic complexity as well as the integration of SNP data into the reconstruction process. Once this is achieved and sufficient curated training data is available, the FST approach allows us to extend our approach to a full probabilistic model of cancer evolution.

## Methods

SNP array data for the example from the OV03/04 study can be accessed at the NCBI Gene Expression Omnibus under accession number *GSE40546*.

### Simulation of tumour evolution

Coalescent trees were simulated using the *APE* R package [41]. Simulation of genome evolution on these trees was performed by custom code, released as the *SimCopy* R package [40]. *SimCopy* relies on the *PhyloSim* package [54] in order to perform the simulations on the level of abstract “genomic regions”. The

genomic regions are encoded in a sequence of integers, with the sign representing their orientation. The package then uses modified *PhyloSim* processes in order to simulate deletion, duplication, inversion, inverted duplication and translocation events happening with rates specified by the user. The number of genomic regions affected by each of these events is modelled by truncated Geometric+1 distributions. After simulating genome evolution, CN profiles are reported for leaf and internal nodes. Genomes were simulated using 15 leaf nodes, a root size of 100 segments and an average event length of 12 segments to allow for overlapping events. Event rates covered the following set: 0.02, 0.03, 0.04, 0.05, 0.07, 0.1, 0.13, 0.15, 0.18, 0.2. Individual event rates were modified with the following factors: deletions: 0.3, duplications: 1.0, inverted duplications: 0.1, inversions: 0.2, translocations: 0.2. All parameters were chosen such that the leaf node CN distributions are similar in shape to CN distributions from experimental data in the clinical study Schwarz *et al.* 2013 (in prep.).

### **Implementation of MEDICC**

All FST and FSA algorithms were implemented using OpenFST [37]. MEDICC was written in Python, while implementation of time-critical parts used C. For the Fitch-Margoliash implementations we used the Phylip package [55]. MEDICC is available at <https://bitbucket.org/rfs/medicc> and has been tested on Windows and UNIX-based systems.

The quantitative analysis of MEDICC results was done in R and all necessary functions are implemented in the *MEDICCquant* package included in the MEDICC distribution. Spatial statistics were computed using the *spatstat* package [49], and for kernel manipulations the *kernelab* package was used [56].

### **Authors contributions**

RFS designed and implemented MEDICC and wrote the ms. AT designed and implemented simulation comparisons with *TuMult*. BS designed and implemented the genome simulations. JDB designed the clinical study and supervised the analysis of clinical data. NG and FM supervised the phylogenetic and machine learning aspects of the project. NG, FM and JDB corrected and edited the ms and all authors approved the final version.

### **Acknowledgements**

The authors would like to thank Gonzalo Iglesias and Adria de Gispert from the Cambridge University Engineering Department for input on the FST implementations. We would further like to thank Eric

Letouze for advice on optimal preparation of our simulated datasets for *TuMult*.

## References

1. Khalique L, Ayhan A, Weale ME, Jacobs IJ, Ramus SJ, Gayther SA: **Genetic intra-tumour heterogeneity in epithelial ovarian cancer and its implications for molecular diagnosis of tumours.** *J Pathol* 2007, **211**(3):286–295, [<http://dx.doi.org/10.1002/path.2112>].
2. Khalique L, Ayhan A, Whittaker JC, Singh N, Jacobs IJ, Gayther SA, Ramus SJ: **The clonal evolution of metastases from primary serous epithelial ovarian cancers.** *Int J Cancer* 2009, **124**(7):1579–1586, [<http://dx.doi.org/10.1002/ijc.24148>].
3. Cooke SL, Ng CKY, Melnyk N, Garcia MJ, Hardcastle T, Temple J, Langdon S, Huntsman D, Brenton JD: **Genomic analysis of genetic heterogeneity and evolution in high-grade serous ovarian carcinoma.** *Oncogene* 2010, **29**(35):4905–4913, [<http://dx.doi.org/10.1038/onc.2010.245>].
4. Navin N, Krasnitz A, Rodgers L, Cook K, Meth J, Kendall J, Riggs M, Eberling Y, Troge J, Grubor V, Levy D, Lundin P, Mánér S, Zetterberg A, Hicks J, Wigler M: **Inferring tumor progression from genomic heterogeneity.** *Genome Res* 2010, **20**:68–80, [<http://dx.doi.org/10.1101/gr.099622.109>].
5. Shah SP, Morin RD, Khattra J, Prentice L, Pugh T, Burleigh A, Delaney A, Gelmon K, Guliany R, Senz J, Steidl C, Holt RA, Jones S, Sun M, Leung G, Moore R, Severson T, Taylor GA, Teschendorff AE, Tse K, Turashvili G, Varhol R, Warren RL, Watson P, Zhao Y, Caldas C, Huntsman D, Hirst M, Marra MA, Aparicio S: **Mutational evolution in a lobular breast tumour profiled at single nucleotide resolution.** *Nature* 2009, **461**(7265):809–813, [<http://dx.doi.org/10.1038/nature08489>].
6. Campbell PJ, Yachida S, Mudie LJ, Stephens PJ, Pleasance ED, Stebbings LA, Morsberger LA, Latimer C, McLaren S, Lin ML, McBride DJ, Varela I, Nik-Zainal SA, Leroy C, Jia M, Menzies A, Butler AP, Teague JW, Griffin CA, Burton J, Swerdlow H, Quail MA, Stratton MR, Iacobuzio-Donahue C, Futreal PA: **The patterns and dynamics of genomic instability in metastatic pancreatic cancer.** *Nature* 2010, **467**(7319):1109–1113, [<http://dx.doi.org/10.1038/nature09460>].
7. Marusyk A, Almendro V, Polyak K: **Intra-tumour heterogeneity: a looking glass for cancer?** *Nat Rev Cancer* 2012, **12**(5):323–334, [<http://dx.doi.org/10.1038/nrc3261>].
8. Navin N, Kendall J, Troge J, Andrews P, Rodgers L, McIndoo J, Cook K, Stepansky A, Levy D, Esposito D, Muthuswamy L, Krasnitz A, McCombie WR, Hicks J, Wigler M: **Tumour evolution inferred by single-cell sequencing.** *Nature* 2011, **472**(7341):90–94, [<http://dx.doi.org/10.1038/nature09807>].
9. Vermaat JS, Nijman IJ, Koudijs MJ, Gerritse FL, Scherer SJ, Mokry M, Roessingh WM, Lansu N, de Bruijn E, van Hillegersberg R, van Diest PJ, Cuppen E, Voest EE: **Primary colorectal cancers and their subsequent hepatic metastases are genetically different: implications for selection of patients for targeted treatment.** *Clin Cancer Res* 2012, **18**(3):688–699, [<http://dx.doi.org/10.1158/1078-0432.CCR-11-1965>].
10. Wu X, Northcott PA, Dubuc A, Dupuy AJ, Shih DJH, Witt H, Croul S, Bouffet E, Fults DW, Eberhart CG, Garzia L, Van Meter T, Zagzag D, Jabado N, Schwartzentruber J, Majewski J, Scheetz TE, Pfister SM, Korshunov A, Li XN, Scherer SW, Cho YJ, Akagi K, MacDonald TJ, Koster J, McCabe MG, Sarver AL, Collins VP, Weiss WA, Largaespada DA, Collier LS, Taylor MD: **Clonal selection drives genetic divergence of metastatic medulloblastoma.** *Nature* 2012, **482**(7386):529–533, [<http://dx.doi.org/10.1038/nature10825>].
11. Nik-Zainal S, Van Loo P, Wedge DC, Alexandrov LB, Greenman CD, Lau KW, Raine K, Jones D, Marshall J, Ramakrishna M, Shlien A, Cooke SL, Hinton J, Menzies A, Stebbings LA, Leroy C, Jia M, Rance R, Mudie LJ, Gamble SJ, Stephens PJ, McLaren S, Tarpey PS, Papaemmanuil E, Davies HR, Varela I, McBride DJ, Bignell GR, Leung K, Butler AP, Teague JW, Martin S, Jönsson G, Mariani O, Boyault S, Miron P, Fatima A, Langerød A, Aparicio SAJR, Tutt A, Sieuwerts AM, Borg Å, Thomas G, Salomon AV, Richardson AL, Børresen-Dale AL, Futreal PA, Stratton MR, Campbell PJ, BCWG/ICGC: **The life history of 21 breast cancers.** *Cell* 2012, **149**(5):994–1007.



12. Gerlinger M, Rowan AJ, Horswell S, Larkin J, Endesfelder D, Gronroos E, Martinez P, Matthews N, Stewart A, Tarpey P, Varela I, Phillimore B, Begum S, McDonald NQ, Butler A, Jones D, Raine K, Latimer C, Santos CR, Nohadani M, Eklund AC, Spencer-Dene B, Clark G, Pickering L, Stamp G, Gore M, Szallasi Z, Downward J, Futreal PA, Swanton C: **Intratumor heterogeneity and branched evolution revealed by multiregion sequencing.** *N Engl J Med* 2012, **366**(10):883–892, [<http://dx.doi.org/10.1056/NEJMoa1113205>].
13. Cooke SL, Temple J, Macarthur S, Zahra MA, Tan LT, Crawford RAF, Ng CKY, Jimenez-Linan M, Sala E, Brenton JD: **Intra-tumour genetic heterogeneity and poor chemoradiotherapy response in cervical cancer.** *Br J Cancer* 2011, **104**(2):361–368, [<http://dx.doi.org/10.1038/sj.bjc.6605971>].
14. Maley CC, Galipeau PC, Finley JC, Wongsurawat VJ, Li X, Sanchez CA, Paulson TG, Blount PL, Risques RA, Rabinovitch PS, Reid BJ: **Genetic clonal diversity predicts progression to esophageal adenocarcinoma.** *Nat Genet* 2006, **38**(4):468–473, [<http://dx.doi.org/10.1038/ng1768>].
15. Park SY, Gönen M, Kim HJ, Michor F, Polyak K: **Cellular and genetic diversity in the progression of in situ human breast carcinomas to an invasive phenotype.** *J Clin Invest* 2010, **120**(2):636–644, [<http://dx.doi.org/10.1172/JCI40724>].
16. Cooke SL, Brenton JD: **Evolution of platinum resistance in high-grade serous ovarian cancer.** *Lancet Oncol* 2011, [[http://dx.doi.org/10.1016/S1470-2045\(11\)70123-1](http://dx.doi.org/10.1016/S1470-2045(11)70123-1)].
17. Ding L, Ellis MJ, Li S, Larson DE, Chen K, Wallis JW, Harris CC, McLellan MD, Fulton RS, Fulton LL, Abbott RM, Hoog J, Dooling DJ, Koboldt DC, Schmidt H, Kalicki J, Zhang Q, Chen L, Lin L, Wendl MC, McMichael JF, Magrini VJ, Cook L, McGrath SD, Vickery TL, Appelbaum E, Deschryver K, Davies S, Guintoli T, Lin L, Crowder R, Tao Y, Snider JE, Smith SM, Dukes AF, Sanderson GE, Pohl CS, Delehaunty KD, Fronick CC, Pape KA, Reed JS, Robinson JS, Hodges JS, Schierding W, Dees ND, Shen D, Locke DP, Wiechert ME, Eldred JM, Peck JB, Oberkfell BJ, Lolofie JT, Du F, Hawkins AE, O’Laughlin MD, Bernard KE, Cunningham M, Elliott G, Mason MD, Thompson DM Jr, Ivanovich JL, Goodfellow PJ, Perou CM, Weinstock GM, Aft R, Watson M, Ley TJ, Wilson RK, Mardis ER: **Genome remodelling in a basal-like breast cancer metastasis and xenograft.** *Nature* 2010, **464**(7291):999–1005, [<http://dx.doi.org/10.1038/nature08989>].
18. Ding L, Ley TJ, Larson DE, Miller CA, Koboldt DC, Welch JS, Ritchey JK, Young MA, Lamprecht T, McLellan MD, McMichael JF, Wallis JW, Lu C, Shen D, Harris CC, Dooling DJ, Fulton RS, Fulton LL, Chen K, Schmidt H, Kalicki-Veizer J, Magrini VJ, Cook L, McGrath SD, Vickery TL, Wendl MC, Heath S, Watson MA, Link DC, Tomasson MH, Shannon WD, Payton JE, Kulkarni S, Westervelt P, Walter MJ, Graubert TA, Mardis ER, Wilson RK, DiPersio JF: **Clonal evolution in relapsed acute myeloid leukaemia revealed by whole-genome sequencing.** *Nature* 2012, **481**(7382):506–510, [<http://dx.doi.org/10.1038/nature10738>].
19. Cowin PA, George J, Fereday S, Loehrer E, Van Loo P, Cullinane C, Etemadmoghadam D, Ftouni S, Galletta L, Anglesio MS, Hendley J, Bowes L, Sheppard KE, Christie EL, AOCs, Pearson RB, Harnett PR, Heinzelmann-Schwarz V, Friedlander M, McNally O, Quinn M, Campbell P, Defazio A, Bowtell DDL: **LRP1B Deletion in High-Grade Serous Ovarian Cancers Is Associated with Acquired Chemotherapy Resistance to Liposomal Doxorubicin.** *Cancer Res* 2012, **72**(16):4060–4073, [<http://dx.doi.org/10.1158/0008-5472.CAN-12-0203>].
20. Network TCGAR: **Integrated genomic analyses of ovarian carcinoma.** *Nature* 2011, **474**(7353):609–615, [<http://dx.doi.org/10.1038/nature10166>].
21. Ng CKY, Cooke SL, Howe K, Newman S, Xian J, Temple J, Batty EM, Pole JCM, Langdon SP, Edwards PAW, Brenton JD: **The role of tandem duplicator phenotype in tumour evolution in high-grade serous ovarian cancer.** *J Pathol* 2012, **226**(5):703–712, [<http://dx.doi.org/10.1002/path.3980>].
22. Greenman CD, Pleasance ED, Newman S, Yang F, Fu B, Nik-Zainal S, Jones D, Lau KW, Carter N, Edwards PAW, Futreal PA, Stratton MR, Campbell PJ: **Estimation of rearrangement phylogeny for cancer genomes.** *Genome Res* 2012, **22**(2):346–361, [<http://dx.doi.org/10.1101/gr.118414.110>].
23. Letouzé E, Allory Y, Bollet MA, Radvanyi F, Guyon F: **Analysis of the copy number profiles of several tumor samples from the same patient reveals the successive steps in tumorigenesis.** *Genome Biol* 2010, **11**(7):R76, [<http://dx.doi.org/10.1186/gb-2010-11-7-r76>].

24. Greenman CD, Bignell G, Butler A, Edkins S, Hinton J, Beare D, Swamy S, Santarius T, Chen L, Widaa S, Futreal PA, Stratton MR: **PICNIC: an algorithm to predict absolute allelic copy number variation with microarray cancer data.** *Biostatistics* 2010, **11**:164–175, [<http://dx.doi.org/10.1093/biostatistics/kxp045>].
25. Korbel JO, Urban AE, Affourtit JP, Godwin B, Grubert F, Simons JF, Kim PM, Palejev D, Carriero NJ, Du L, Taillon BE, Chen Z, Tanzer A, Saunders ACE, Chi J, Yang F, Carter NP, Hurles ME, Weissman SM, Harkins TT, Gerstein MB, Egholm M, Snyder M: **Paired-end mapping reveals extensive structural variation in the human genome.** *Science* 2007, **318**(5849):420–426, [<http://dx.doi.org/10.1126/science.1149504>].
26. Yoon S, Xuan Z, Makarov V, Ye K, Sebat J: **Sensitive and accurate detection of copy number variants using read depth of coverage.** *Genome Res* 2009, **19**(9):1586–1592, [<http://dx.doi.org/10.1101/gr.092981.109>].
27. Felsenstein J: *Inferring phylogenies.* Sinauer Associates 2003.
28. Levenshtein V: **Binary codes capable of correcting deletions, insertions, and reversals.** *Soviet Physics - Doklady* 1966, **10**:707–710.
29. Mohri M: **Edit-Distance of Weighted Automata: General Definitions and Algorithms.** *IJFCS* 2003, **14**(6):957–982.
30. Mohri M: *Weighted Finite-State Transducer Algorithms An Overview,* Physica-Verlag 2004 .
31. Droste M, Kuich W, Vogler H (Eds): *Handbook of Weighted Automata,* Springer 2009 chap. Weighted Automata Algorithms, :1–45.
32. Durbin R, Eddy S, Krogh A, Mitchison G: *Biological Sequence Analysis.* Cambridge University Press 1998.
33. Schwarz RF, Fletcher W, Förster F, Merget B, Wolf M, Schultz J, Markowetz F: **Evolutionary distances in the twilight zone—a rational kernel approach.** *PLoS One* 2010, **5**(12):e15788, [<http://dx.doi.org/10.1371/journal.pone.0015788>].
34. Felsenstein J: **Evolutionary trees from DNA sequences: a maximum likelihood approach.** *J Mol Evol* 1981, **17**(6):368–376.
35. Corinna Cortes, Patrick Haffner, Mehryar Mohri: **Rational Kernels: Theory and Algorithms.** *JMLR* 2004, **1**:1–50.
36. Shawe-Taylor J, Cristianini N: *Kernel Methods for Pattern Analysis.* Cambridge University Press 2004.
37. Allauzen C, Riley M, Schalkwyk J, Skut W, Mohri M: **OpenFst: A General and Efficient Weighted Finite-State Transducer Library.** *Proceedings of the Ninth International Conference on Implementation and Application of Automata, (CIAA), in Lecture Notes in Computer Science* 2007, **4783**:11–23.
38. Allauzen C, Riley M: **A Pushdown Transducer Extension for the OpenFst Library.** In *CIAA, Volume 7381 of Lecture Notes in Computer Science.* Edited by Moreira N, Reis R, Springer 2012:66–77, [<http://dblp.uni-trier.de/db/conf/wia/ciaa2012.html#AllauzenR12>].
39. Fitch WM, Margoliash E: **Construction of phylogenetic trees.** *Science* 1967, **155**(3760):279–284.
40. Sipos B: **SimCopy - a R package simulating the evolution of copy number profiles along a tree** 2013, [<https://github.com/sbotond/simcopy>].
41. Paradis E, Claude J, Strimmer K: **APE: Analyses of Phylogenetics and Evolution in R language.** *Bioinformatics* 2004, **20**(2):289–290.
42. Gascuel O: **BIONJ: an improved version of the NJ algorithm based on a simple model of sequence data.** *Mol Biol Evol* 1997, **14**(7):685–695.

43. Mailund T, Pedersen CNS: **QDist—quartet distance between evolutionary trees.** *Bioinformatics* 2004, **20**(10):1636–1637, [<http://dx.doi.org/10.1093/bioinformatics/bth097>].
44. Schölkopf B, Smola A, Müller KR: **Nonlinear Component Analysis as a Kernel Eigenvalue Problem.** *Neural Computation* 1998, **10**(5):1299–1319, [<http://dx.doi.org/10.1162/089976698300017467>].
45. Smith JM, Smith NH, O’Rourke M, Spratt BG: **How clonal are bacteria?** *Proceedings of the National Academy of Sciences* 1993, **90**(10):4384–4388, [<http://www.pnas.org/content/90/10/4384.abstract>].
46. Hartl DL, Clark AG: *Principles of Population Genetics.* Sinauer Associates 2007.
47. Besag J: **Contribution to the discussion of Dr Ripley’s paper.** *Journal of the Royal Statistical Society* 1977, **Series B**, **39**:193–195.
48. Ripley B: **Modelling spatial patterns (with discussion).** *Journal of the Royal Statistical Society* 1977, **Series B**, **39**:172–212.
49. Baddeley A, Turner R: **Spatstat: an R package for analyzing spatial point patterns.** *Journal of Statistical Software* 2005, **12**(6):1–42, [[www.jstatsoft.org](http://www.jstatsoft.org)]. [ISSN 1548-7660].
50. Adams JM, Strasser A: **Is tumor growth sustained by rare cancer stem cells or dominant clones?** *Cancer Res.* 2008, **68**(11):4018–4021.
51. Sala E, Kataoka MY, Priest AN, Gill AB, McLean MA, Joubert I, Graves MJ, Crawford RAF, Jimenez-Linan M, Earl HM, Hodgkin C, Griffiths JR, Lomas DJ, Brenton JD: **Advanced ovarian cancer: multiparametric MR imaging demonstrates response- and metastasis-specific effects.** *Radiology* 2012, **263**:149–59.
52. van de Wiel MA, van Wieringen WN: **CGHregions: dimension reduction for array CGH data with minimal information loss.** *Cancer Inform* 2007, **3**:55–63.
53. Archibald KM, Kulbe H, Kwong J, Chakravarty P, Temple J, Chaplin T, Flak MB, McNeish IA, Deen S, Brenton JD, Young BD, Balkwill F: **Sequential genetic change at the TP53 and chemokine receptor CXCR4 locus during transformation of human ovarian surface epithelium.** *Oncogene* 2012, **31**(48):4987–4995, [<http://dx.doi.org/10.1038/onc.2011.653>].
54. Sipos B, Masingham T, Jordan GE, Goldman N: **PhyloSim - Monte Carlo simulation of sequence evolution in the R statistical computing environment.** *BMC Bioinformatics* 2011, **12**:104, [<http://dx.doi.org/10.1186/1471-2105-12-104>].
55. Felsenstein J: **PHYLIP (Phylogeny Inference Package) version 3.6.** Distributed by the author. Department of Genome Sciences, University of Washington, Seattle. 2009.
56. Karatzoglou A, Smola A, Hornik K, Zeileis A: **kernlab – An S4 Package for Kernel Methods in R.** *Journal of Statistical Software* 2004, **11**(9):1–20, [<http://www.jstatsoft.org/v11/i09/>].

## Figures

Figure 1 - Evolutionary CN trees are reconstructed in three steps

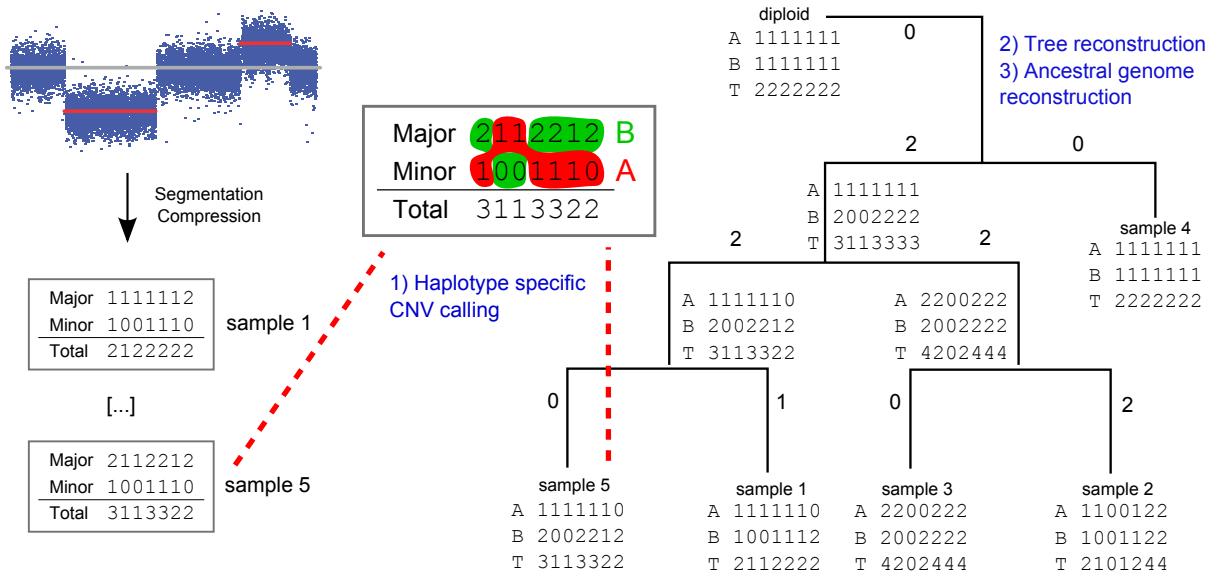


Figure 1: **Evolutionary CN trees are reconstructed in three steps:** 1) After segmentation and compression, major and minor alleles are phased using the minimum event criterion. 2) The tree topology is reconstructed from the pairwise distances between genomes. 3) Reconstruction of ancestral genomes yields the final branch lengths of the tree, which correspond to the number of events between genomes.

Figure 2 - Efficient distance calculation is enabled via a transducer architecture

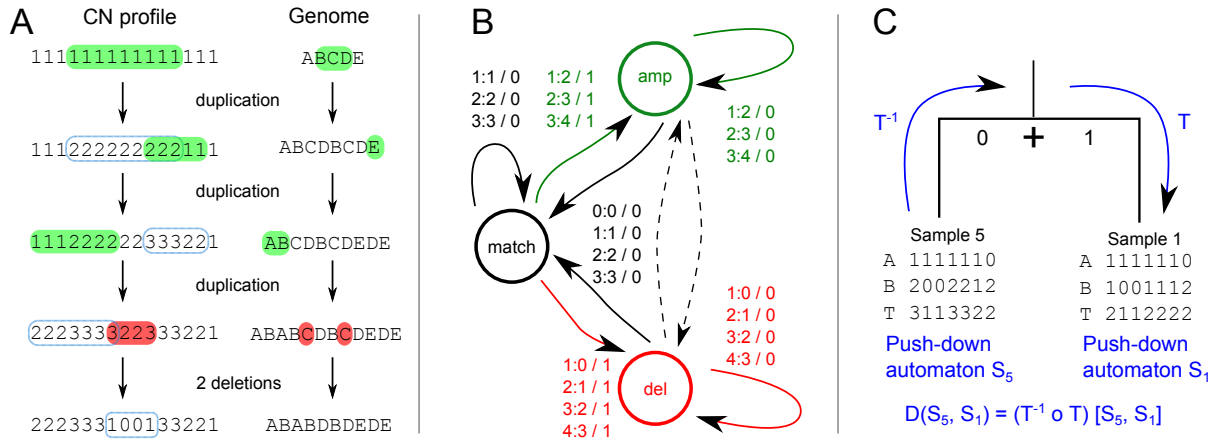


Figure 2: **Efficient distance calculation is enabled via a transducer architecture:** A) Overlapping genomic rearrangements modify the associated CN profiles in different ways. Amplifications are indicated in green, deletions in red. The blue rectangles indicate the previous event. B) The one-step minimum event transducer describes all possible edit operations achievable in one event. This FST is composed  $n$  times with itself to create the full minimum event FST  $T$ . Edge labels consist of an input symbol, a colon and the corresponding output symbol, followed by a slash and the weight associated with taking that transition. C) The minimum event FST  $T$  is asymmetric and describes the evolution of a genomic profile from its ancestor. Composed with its inverse this yields the symmetric minimum event distance  $D$ .

Figure 3 - Parental alleles are phased using context-free grammars

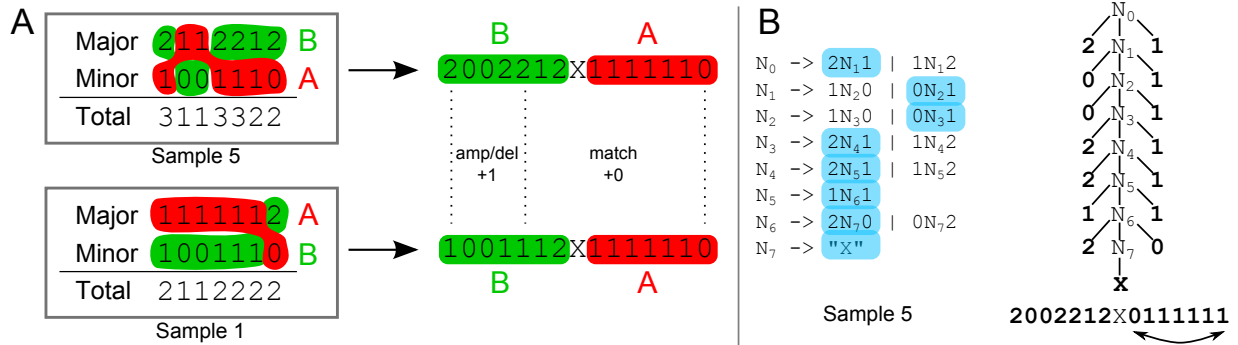
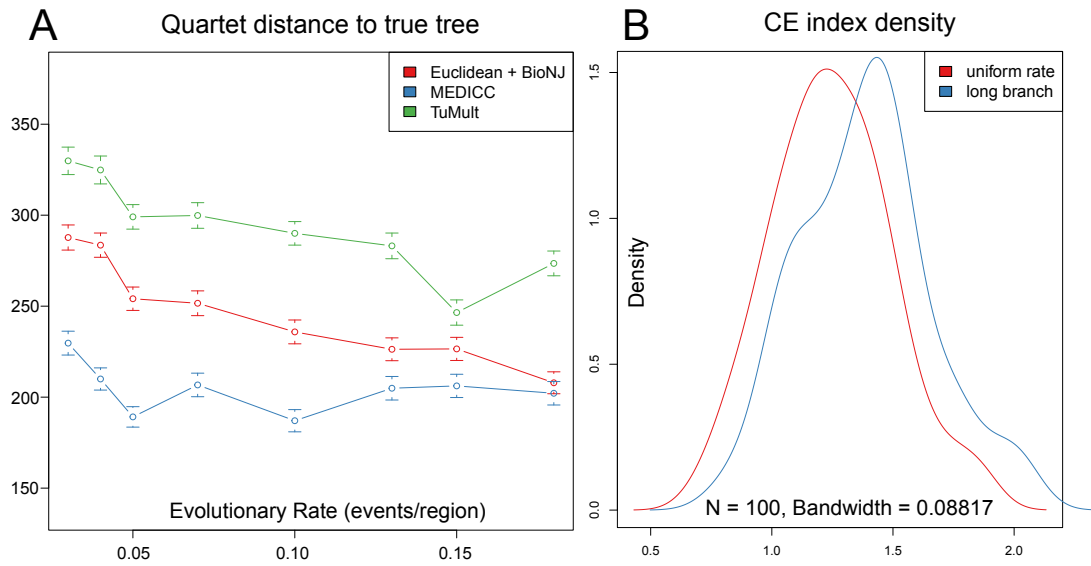


Figure 3: **Parental alleles are phased using context-free grammars:** A) Allelic phasing is achieved by choosing consecutive segments from either the major or minor allele which minimise the pairwise distance between profiles. B) The set of all possible phasing choices is modelled by a context-free grammar. In this representation, the order of the regions' CN values on the second allele is reversed, in order to match the inside-out parsing scheme of CFGs. That way every possible parse tree of the grammar describes one possible phasing.

**Figure 4 - MEDICC improves reconstruction accuracy over competing methods**



**Figure 4: MEDICC improves reconstruction accuracy over competing methods:** A) Simulations results show the improvement of reconstruction accuracy for MEDICC over naive methods (BioNJ clustering on Euclidean distances between CN profiles, red) and competing algorithms (TuMult, green). B) Density estimates of clonal expansion indices for neutrally evolving trees (red) and trees with induced long branches as created by clonal expansion processes (blue) show the ability of MEDICC to detect clonal expansion.

Figure 5 - MEDICC quantifies ITH from the locations of genomes on the mutational landscape

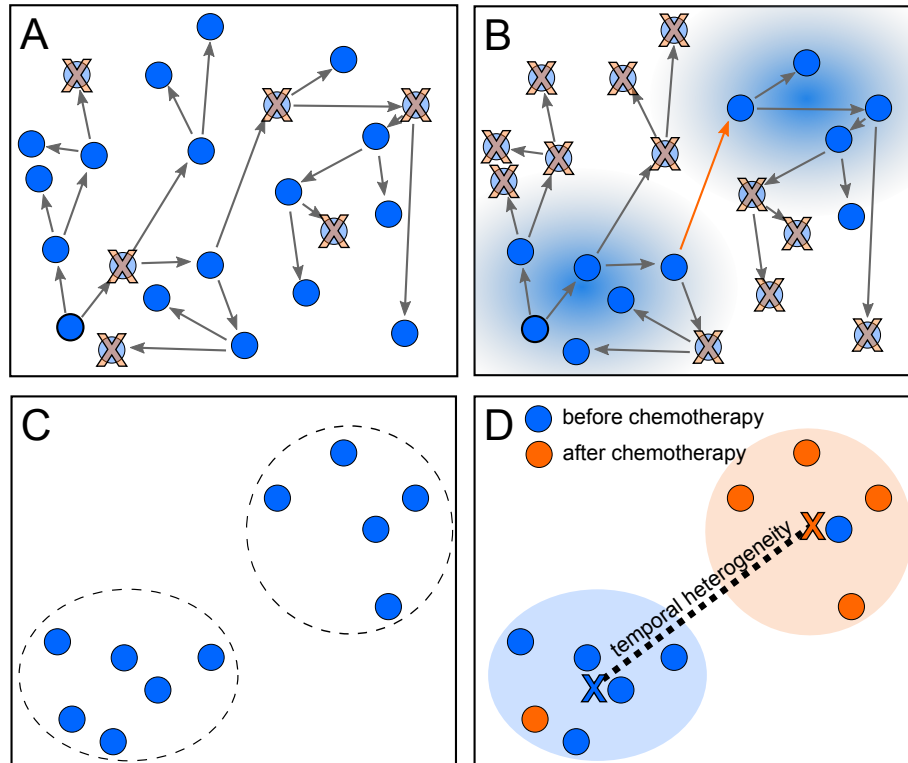


Figure 5: **MEDICC quantifies ITH from the locations of genomes on the mutational landscape:** A) If no or a homogeneous selection pressure is applied, cells proliferate and die randomly across the mutational landscape, leaving the surviving cells spatially unclustered. B) If the fitness landscape favours specific mutations (blue shaded areas), genomes inside those areas are more likely to survive, those outside more likely to die. The ability of a tumour for a clonal expansion into distant fitness pockets depends on its mutation potential per generation (long orange arrow). This leads to C) a situation where distinct subpopulations/clonal expansions are present in a tumour, indicating a generally high potential for a tumour to adapt to changing environments. D) The mutational landscape additionally allows estimates of average distance between two subgroups of samples, here before (blue) and after (orange) chemotherapy. The distance between the two subgroups is defined as the distance of the robust centres of mass (blue and orange X). This robust centre of mass is computed omitting the single most distant point of each subgroup (blue and orange samples in the orange and blue subgroups respectively), making the statistic more resistant towards outliers.



Figure 6 - Application to a case of endometrioid cancer

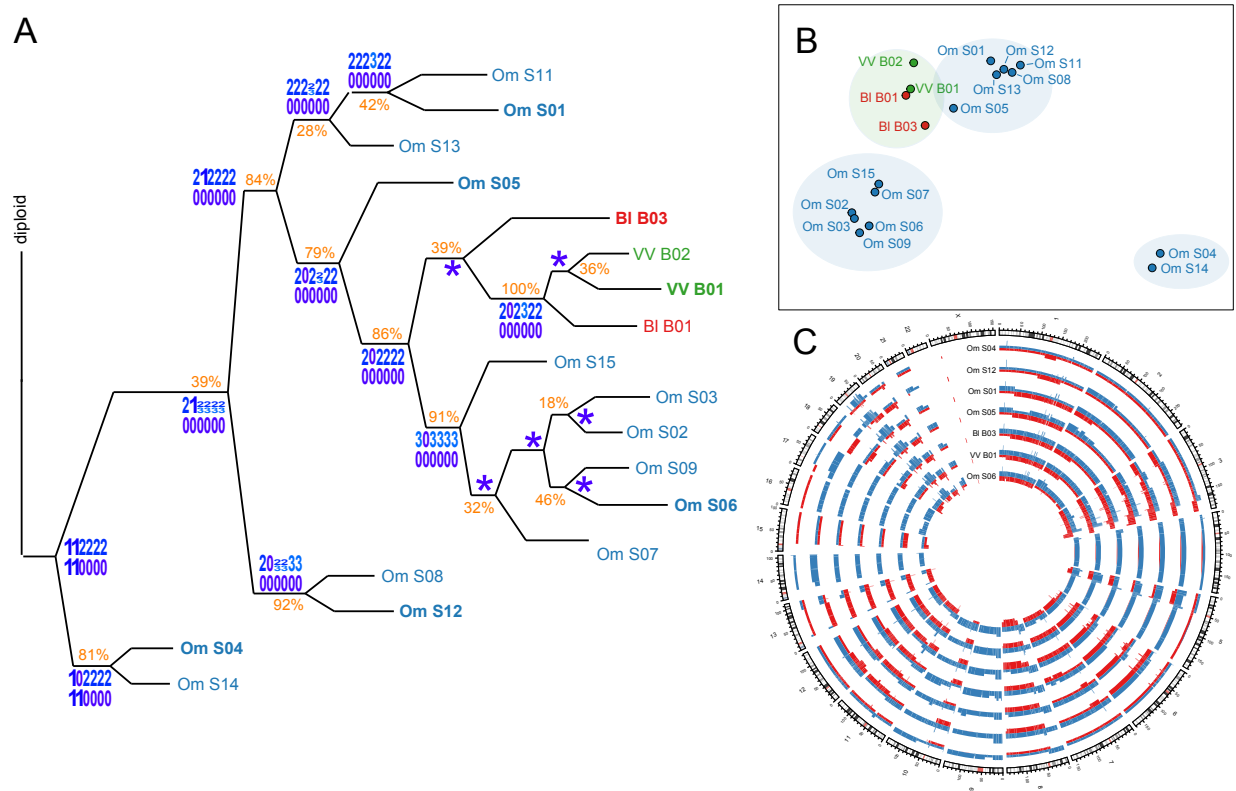


Figure 6: **Application to a case of endometrioid cancer:** A) Evolutionary tree of the OV03-04 case reconstructed from whole genome CN profiles. Approximate support values indicate how often each split was observed in trees reconstructed after resampling of the distance matrix with added truncated Gaussian noise. MEDICC performs reconstruction of ancestral CN profiles. Here, the (compressed) ancestral profiles for chromosome 17 are given as an example and MEDICC depicts unresolved ambiguities in the form of sequence logos. A star indicates no change compared to its ancestor. B) Ordination of the samples using kPCA shows four clear clonal expansions, comprising three separate Omentum groups and the BI/VV group. C) Circos plot of selected genomic profiles (marked in bold in the tree) shows the extent of chromosomal aberrations across the genome. The two phased parental alleles are indicated in red and blue.